Three-dimensional measurements of deformable oil droplets in turbulence

Leonel E. Beckedorff[1], Giuseppe C.A. Caridi[1,*], Alfredo Soldati[1,2]

1: Institute of Fluid Mechanics and Heat Transfer,TUWien,Austria
2: Polytechnic Department, University of Udine, Italy
*Corresponding author: giuseppe.caridi@tuwien.ac.at

Keywords: 3D time-resolved droplet reconstruction, Shake-the-Box, HIT facility.

ABSTRACT

This work introduces an experimental facility designed to generate turbulence with a high energy dissipation rate of up to 0.3 m^2s^{-3}, sufficient to induce deformation and fragmentation of oil droplets. The turbulence is produced by opposing arrays consisting of 24 jet streams in total, each with Reynolds numbers ranging from 12,000 to 50,000. Flow regimes are determined using 3D Particle Tracking Velocimetry (PTV) conducted in the center of the octagonal test section. The statistical analysis of the turbulence reveals a nearly homogeneous and isotropic nature. A 3D imaging system, equipped with six high-speed cameras, allows for the reconstruction of droplets using the multiple algebraic reconstruction technique algorithm, fostering both visualization and quantification of interface deformation. Additionally, the system enables the tracking of the breakup process. The presented setup is able to couple the measurements of the droplet shapes with surrounding turbulence in 3D dproplet topology reconstruction coupled with surrounding flow measurements. We demonstrate the capability of our imaging system and reconstruction methods for multiphase flow studies with an example of full 3D droplet topology reconstruction coupled with surrounding flow measurements.

1. Introduction

In the pursuit of a comprehensive understanding of turbulent flows and their implications for multiphase systems, this work introduces an experimental facility dedicated to the study of controlled turbulence at high dissipation rates (ε). In the past, various facilities have been constructed to investigate high Reynolds numbers, including traditional wind tunnels, water tunnels, coaxial counter-rotating disk systems, and Taylor-Couette setups, among others. Despite the extensive focus on achieving high Reynolds numbers over the decades, the impact of the high energy dissipation rate has received less attention, even though it holds greater significance than Re in multiphase flows (Masuk, Salibindla, Tan, & Ni, 2019). In particular, deformation and fragmentation of droplets is influenced by small-scale local flow structures governed by ε. The combination of controlled turbulence, high dissipation rates, and advanced three-dimensional imaging techniques

marks a significant advancement to unravel the nuances of multiphase flows, particularly shedding light on the behavior of oil droplets under dynamic conditions.
We introduce a jet facility designed to investigate the changes in topology of droplets and bubbles dispersed in homogeneous isotropic turbulence (HIT). If ϵ is high, it means the turbulent pressure fluctuations are strong enough to overcome the interfacial tension and cause the droplet to break apart. However, if the droplets have a high internal viscosity, they can better resist these interfacial deformations. Consequently, droplets with higher viscosity require even higher values of ϵ to break. In addition, the breakup is driven by eddies of similar size to the droplet diameter (Ni, 2023). Although the last assumption has been challenged recently (Qi et al., 2022; Vela-Martín & Avila, 2021). In the end, the breakage of droplets and bubbles by turbulence is a critical phenomenon that still demands a thorough understanding (Deike, 2022; Ni, 2023; Vela-Martín & Avila, 2022). The findings demonstrate that, under these specific flow conditions, neutrally buoyant oil droplets can undergo deformation and breakage within the controlled volume for an extended duration. The employment of a state-of-the-art 3D time-resolved imaging system, specifically a Particle Image Velocimetry (PIV) setup with six high-speed cameras, enables to generate a homogeneous source of data that can lead to further investigation on this problem of fundamental importance for a number of industrial and environmental applications.
In this study, we describe a novel octagonal water tank designed to generate intense turbulence using two opposing jet arrays operating in continuous flow. This facility can achieve exceptional Re_λ and ϵ values while maintaining high isotropy and minimal mean flow. By adjusting the jet velocities and the distance between the jet arrays, we can use ϵ scaling and decay to optimize the turbulence characteristics at the tank's center. This setup is ideal for our primary objective of studying droplet deformation and breakup in homogeneous isotropic turbulence (HIT). It allows us to explore a broad range of droplet internal viscosities and Weber numbers (We) while adhering to the key assumptions of the Kolmogorov-Hinze framework. Additionally, although our focus is on droplets in turbulence, this new facility is suitable for a variety of single-phase and multiphase flow applications.

2. Experimental apparatus

The experiments were carried out in a water loop featuring a centrifugal pump (5.5 kW) with a nominal power of 6.5 kW, capable of circulating up to 18 m^3/h of unloaded water. The schematic of the facility is illustrated in the figure 1. The test section was constructed from 25 mm thick cast acrylic in an octagonal shape to facilitate optical access, with a hydraulic diameter of approximately 21 cm. Figure 1(a) illustrates the octagonal tank. We had 80 cm of optical access in the central section. A window in the top center section was included for placing a calibration target in the tank. Turbulence was generated by two opposing jet arrays connected to the ends of the test section. Each array consisted of 12 rigid pipes 0f 6 mm diameter. Each jet released flow with an initial velocity (V_{jet}) ranging from 2 to 14 m/s, resulting in jet Reynolds numbers (Re_{jet}) from 12,000 to 100,000. The relatively high velocity was necessary to generate a high turbulent energy

dissipation rate and increase the probability of droplet breakup. Under the region of interest, at the center of the test section, is placed the needle used to inject the oil droplets.

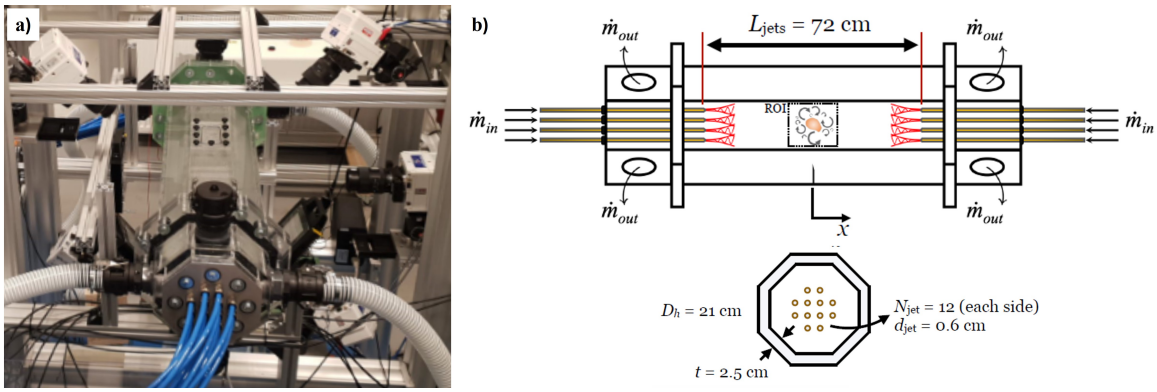

Figure 1. a) Picture of the experimental set-up with test section imaging system. b) Schematic of the test section.

The image acquisition consisted of six high-speed cameras model Phantom VEO 340L, with resolution of 2560×1600 pixels and 10 μm pixel pitch. The cameras were equipped with 100 mm focal length Tokina macro objective and mounted in Scheimpflug condition. The optical magnification was approximately 0.6 and the extent of the measured domain was approximately 4×4×4 cm^3. Throughout this work, we used four cameras to retrieve the single-phase turbulence statistics (setup shown in Figure **??**). The setup with six cameras is recommended for the two-phase measurements: using more cameras allows capturing more tracers near the interface (Masuk, Salibindla, Tan, & Ni, 2019) and fosters better quality of the 3D shape reconstruction (Masuk, Salibindla, & Ni, 2019). Image acquisition and processing was done using the LaVision software DaVis 10.2.1.

We used different illumination systems for the single- and two-phase cases. For single-phase measurements, we used a dual-cavity laser Nd:YAG Litron LD25- 527, synchronized with the cameras by a LaVision Programmable Timing Unit X (PTU X). For the two-phase case, we used dedicated LEDs from PHLOX (HSC Backlight) opposing each camera. The first setup was advantageous for the LPT —we were able to detect more particle trajectories per unity of volume. However, the laser was inadequate for droplet visualization as the interfaces reflected the laser sheet and cast shadows in the measurement volume. With the backlight system, one can obtain a sharper projection of the droplets silhouette and still track the particles shadows (Chang et al., 2023; Masuk, Salibindla, Tan, & Ni, 2019).

In both cases, the water was seeded with 20 μm polyamide particles (1.03 g/cm^3 density). The ratio between particle diameter and the Kolmogorov length scale, η, was of $\mathcal{O}$(0.1–1). The seeding particles could be treated as tracers as their response time were much smaller than the Kolmogorov time scale, τ_η ($St \approx 8 \times 10^{-4}$, where the Stokes number is the ratio between particle response time and τ_η Raffel et al. (2018)). The laser sheet illuminated the seeding particles from the test section bottom wall, entering with an angle to deviate from the droplet injection components. We used a set of lenses and mirrors to adjust the sheet thickness to about 4 cm and illuminate the tank center.

The two different measurements were conducted within similar measurement volumes: Single-phase velocity data were obtained using 3D-LPT with the Shake-The-Box method Schanz et al. (2016). The 3D interface topology was determined using the multiplicative algebraic reconstruction technique (MART) algorithm Elsinga et al. (2006). For single-phase velocity statistics, we acquired 1000 loops of 50 consecutive frames using the recording-loop mode in DaVis to ensure the convergence of the turbulent quantities (from 5000 to 10000 trajectories were identified per frame). Flow rate and temperature data were simultaneously recorded. We repeated the VSC after every 200 loops to preserve a precise calibration. The raw particle images were then pre-processed in DaVis with a sliding minimum subtraction and a spatial normalization with the local average. We obtained the particle trajectories with the STB method, setting the allowed triangulation to 1.0 voxel and adding a second pass (backward in time) to complement the tracks Schröder & Schanz (2023). The data were exported from DaVis and post-processed in an in-house binning MATLAB code for the single-point statistics or used in the Lagrangian form for the two-point statistics.

To obtain time-resolved and averaged statistics on the droplets dynamics, we needed to simultaneously reconstruct the droplet topology and identify the surrounding flow structures with the 3D-LPT. These experiments were conducted with six high-speed cameras and the backlight illumination system. The acquired images were pre-processed to segment droplets and surrounding particles. We then used the MART algorithm in DaVis 10.2.1 to retrieve the interface shape and STB for the particle trajectories. The MART data were exported to an in-house MATLAB code and converted to a volumetric binary image. The volume of the droplets was obtained by counting the number of voxels of each 3D object.

3. Turbulence assessment

The instantaneous velocity field, denoted as U_i, was decomposed into the temporal mean velocity ($\overline{U_i}$) and the fluctuation velocity (u_i), represented as $U_i = \overline{U_i} + u_i$. Here, the subscripts $i = (1, 2, 3)$ correspond to the directions (x, y, z), and $\langle ... \rangle$ denotes ensemble averaging. Figure 2 illustrates the variation of $\overline{U_i}$ and the root mean square of fluctuation velocity, $u_i' = \langle u_i^2 \rangle^{1/2}$, along the x and y axes. Although not shown here, similar trends were observed along the z-direction. The experiment was conducted with $V_{\text{jet}} = 8$ m/s, $N = 12$. The velocity profiles indicated a region of homogeneous turbulence extending over a volume of at least $4 \times 4 \times 4$ cm^3. Additionally, the mean velocities were found to be less than 10% of the corresponding fluctuations.

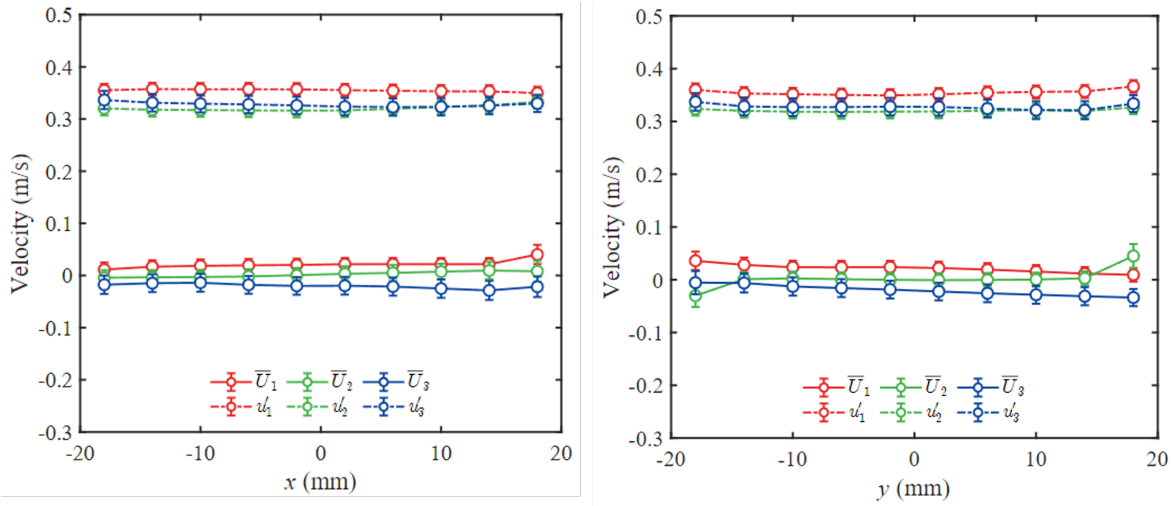

Figure 2. Mean velocity and root-mean-squared fluctuation velocity profiles along the (left) x-direction and (right) y-direction. The jet array configuration was: $N = 12$, $d = 6$ mm, $V_{\text{jet}} = 8$ m/s. Indexes $i = 1, 2, 3$ stand for x, y, and z.

The velocity profiles indicated the presence of a homogeneous turbulence region spanning a volume of at least $4 \times 4 \times 4$ cm^3. Additionally, the mean velocities were observed to be less than 10% of the respective fluctuations. The strength of the mean flow can be further assessed by calculating the ratio of its kinetic energy to the average turbulent kinetic energy, denoted as $m^* = (\overline{U} \cdot \overline{U})/(u_1'^2 + u_2'^2 + u_3'^2)$ Variano & Cowen (2008). Variano and Cowen (Variano & Cowen, 2008) proposed that mean flow effects are insignificant when $m^* < 5\%$. In conjunction with the homogeneity condition, the turbulence should ideally be isotropic. For the setup reported in Fig. 2, the isotropy ratios were $u_1'/u_2' = 1.09$ and $u_2'/u_3' = 0.98$. These values were similar to the ones from Bellani and Variano Bellani & Variano (2013).

We derived the energy dissipation rate using the second-order structure functions, namely $D_{LL}(r) = \langle [u_\parallel(x+r) - u_\parallel(x)]^2 \rangle$ and $D_{NN}(r) = \langle [u_\perp(x+r) - u_\perp(x)]^2 \rangle$. To compute D_{LL} and D_{NN} from the Lagrangian particle trajectories, we defined r as the separation between a given pair of particles and projected their velocities parallel, $u_\parallel$, and perpendicular, $u_\perp$, to the r-direction (Masuk et al., 2021; Qi et al., 2022). For each time instant containing n tracked particles, we identified up to $n(n-1)/2$ pairs of particles, covering a wide range of r and ensuring convergence of the ensemble-averaged quantities. Subsequently, we utilized the scaling laws of the inertial range to deduce ϵ from the second-order structure functions.

$$\epsilon = \frac{(D_{LL}/C_2)^{3/2}}{r} = \frac{(\frac{3}{4}D_{NN}/C_2)^{3/2}}{r} \tag{1}$$

The Kolmogorov constant spans from 2 to 2.2. Here we adopted $C_2 = 2.13$. In Figure 3-left, we present the second-order structure functions for both low and high-end cases, alongside the corresponding energy dissipation rates measured under homogeneous isotropic turbulence (HIT) conditions. Both cases were obtained using the same experimental setup as depicted in Figure 2, with variations in velocity ($V_{\text{jet}} = 2$ and 8 m/s). While the dissipative range couldn't be resolved, the resolution allowed for solving around 10η and capturing the inertial range plateau ($\eta \ll r \ll$

L). In the case of the higher ϵ, the integral-to-Kolmogorov length scale ratio was approximately 1500.

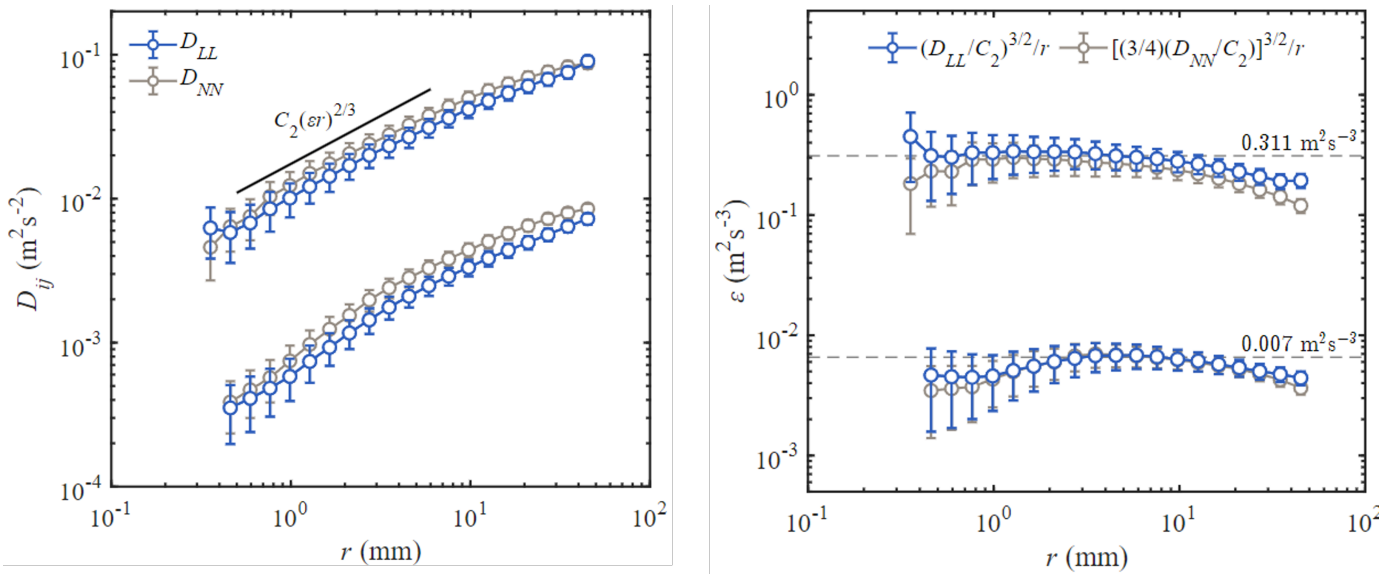

Figure 3. Second-order structure functions (left) and respective energy dissipation rates (right) based on the scaling laws . The jet array configuration was: $N = 12$, $d = 6$ mm, $M = 3.1$ cm, S = 72 cm. Low and high values were obtained with $V_{\text{jet}} = 2$ m/s and $V_{\text{jet}} = 8$ m/s. The plateau in the ϵ profile indicated the inertial range.

The ϵ profiles illustrated in Figure 3-right were distinctly separated by nearly two order of magnitude, underscoring that the average turbulence intensity can be adjusted based on the specific analysis, such as droplet breakup or deformation. Moreover, in an array configuration with $N = 4$ and $V_{\text{jet}} = 14$ m/s, we achieved $\epsilon > 1$ m^{2}s^{-3}, albeit with elevated anisotropy and inhomogeneity. In this scenario, even with an acquisition frequency of 4 kHz, the average particle displacement remained relatively high ($\sim 20; \overline{px}$), potentially compromising the accuracy of the Shake-The-Box method Schanz et al. (2016).

4. Droplet deformation

The deformation and fragmentation of three different nearly neutrally buoyant oil droplets with dynamic viscosity ratios (dispersed over the carrier phase) of 0.65, 20, and 1000, are presented. Figure 4 depicts the viscous effects during the breakup process at the same flow regime (Re$_{jet}$=50·10^3) and for the same initial bubble size (d_d=4mm). In particular, significant stretching of fluid particles. The amount of stretching increases with rising droplet viscosity, as documented in the litterature [Eastwood et al. (2004); Ni (2023)]. An example of the droplet reconstruction for μ_d/μ_c=1000 during the breakup is shown in figure 5(a). While in figure 5(b), is presented the two-phases reconstruction obtained coupling the droplet reconstructed with MART algorithm and the trajectories of the tracers obtained with shake-the-box.

Figure 4. Droplet deformation few instants before the breakup occurred for the different oils with dynamic viscosity ratios (dispersed over the carrier phase) μ_d/μ_c=0.65 (a), μ_d/μ_c=20 (b), and μ_d/μ_c=1000 (c) for Re_{jet}=50·10^3.

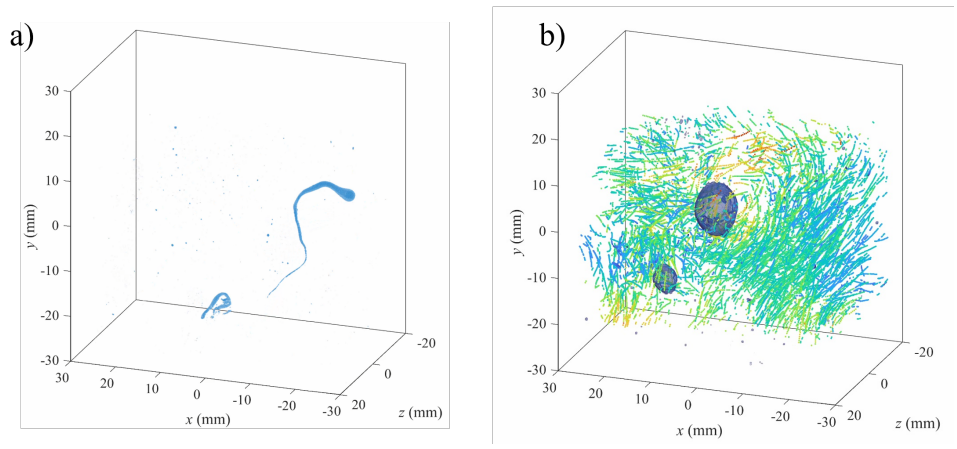

Figure 5. a) Three-dimensional reconstruction of a oil droplet with μ_d/μ_c=1000 using MART algorithm. (b) Reconstructed droplet with surrounding tracer particle trajectories color coded by their velocity magnitude.

5. Conclusion

We have demonstrated that the facing jet array configuration generates homogeneous turbulence with minimal anisotropy in the central region of the facility, covering a volume suitable for tracking and characterizing the interfaces of discrete phases. Specifically, the apparatus can operate at Reynolds numbers up to 800, with anisotropy levels around 10%. The turbulence fluctuations generated are high enough to break the oil droplets. inally, we provided an example of droplet topology reconstruction combined with particle tracking under HIT conditions, confirming the capability of this new facility for multiphase flow measurements.

References

Bellani, G., & Variano, E. A. (2013, December). Homogeneity and isotropy in a laboratory turbulent flow. *Experiments in Fluids*, *55*(1). Retrieved from `http://dx.doi.org/10.1007/s00348-013-1646-8` doi: 10.1007/s00348-013-1646-8

Chang, Y., Müller, C., Kováts, P., Guo, L., & Zähringer, K. (2023, December). Hydrodynamics and shape reconstruction of single rising air bubbles in water using high-speed tomo-

graphic particle tracking velocimetry and 3d geometric reconstruction. *Experiments in Fluids*, *65*(1). Retrieved from http://dx.doi.org/10.1007/s00348-023-03746-0 doi: 10.1007/s00348-023-03746-0

Deike, L. (2022, January). Mass transfer at the ocean–atmosphere interface: The role of wave breaking, droplets, and bubbles. *Annual Review of Fluid Mechanics*, *54*(1), 191–224. Retrieved from http://dx.doi.org/10.1146/annurev-fluid-030121-014132 doi: 10.1146/annurev-fluid-030121-014132

Eastwood, C. D., Armi, L., & Lasheras, J. (2004). The breakup of immiscible fluids in turbulent flows. *Journal of Fluid Mechanics*, *502*, 309–333.

Elsinga, G. E., Scarano, F., Wieneke, B., & van Oudheusden, B. W. (2006, October). Tomographic particle image velocimetry. *Experiments in Fluids*, *41*(6), 933–947. Retrieved from http://dx.doi.org/10.1007/s00348-006-0212-z doi: 10.1007/s00348-006-0212-z

Masuk, A. U. M., Salibindla, A., & Ni, R. (2019, November). A robust virtual-camera 3d shape reconstruction of deforming bubbles/droplets with additional physical constraints. *International Journal of Multiphase Flow*, *120*, 103088. Retrieved from http://dx.doi.org/10.1016/j.ijmultiphaseflow.2019.103088 doi: 10.1016/j.ijmultiphaseflow.2019.103088

Masuk, A. U. M., Salibindla, A., Tan, S., & Ni, R. (2019). V-onset (vertical octagonal noncorrosive stirred energetic turbulence): a vertical water tunnel with a large energy dissipation rate to study bubble/droplet deformation and breakup in strong turbulence. *Review of Scientific Instruments*, *90*(8).

Masuk, A. U. M., Salibindla, A. K., & Ni, R. (2021, March). The orientational dynamics of deformable finite-sized bubbles in turbulence. *Journal of Fluid Mechanics*, *915*. Retrieved from http://dx.doi.org/10.1017/jfm.2021.69 doi: 10.1017/jfm.2021.69

Ni, R. (2023). Deformation and breakup of bubbles and drops in turbulence. *Annual Review of Fluid Mechanics*, *56*.

Qi, Y., Tan, S., Corbitt, N., Urbanik, C., Salibindla, A. K. R., & Ni, R. (2022, January). Fragmentation in turbulence by small eddies. *Nature Communications*, *13*(1). Retrieved from http://dx.doi.org/10.1038/s41467-022-28092-3 doi: 10.1038/s41467-022-28092-3

Raffel, M., Willert, C. E., Scarano, F., Kähler, C. J., Wereley, S. T., & Kompenhans, J. (2018). *Particle image velocimetry: A practical guide*. Springer International Publishing. Retrieved from http://dx.doi.org/10.1007/978-3-319-68852-7 doi: 10.1007/978-3-319-68852-7

Schanz, D., Gesemann, S., & Schröder, A. (2016). Shake-the-box: Lagrangian particle tracking at high particle image densities. *Experiments in fluids*, *57*, 1–27.

Schröder, A., & Schanz, D. (2023, January). 3d lagrangian particle tracking in fluid mechanics. *Annual Review of Fluid Mechanics*, *55*(1), 511–540. Retrieved from http://dx.doi.org/10.1146/annurev-fluid-031822-041721 doi: 10.1146/annurev-fluid-031822-041721

Variano, E. A., & Cowen, E. A. (2008, May). A random-jet-stirred turbulence tank. *Journal of Fluid Mechanics*, *604*, 1–32. Retrieved from http://dx.doi.org/10.1017/S0022112008000645 doi: 10.1017/s0022112008000645

Vela-Martín, A., & Avila, M. (2021, October). Deformation of drops by outer eddies in turbulence. *Journal of Fluid Mechanics*, *929*. Retrieved from http://dx.doi.org/10.1017/jfm.2021.879 doi: 10.1017/jfm.2021.879

Vela-Martín, A., & Avila, M. (2022, December). Memoryless drop breakup in turbulence. *Science Advances*, *8*(50). Retrieved from http://dx.doi.org/10.1126/sciadv.abp9561 doi: 10.1126/sciadv.abp9561